A computational study of twist boundary structures in strontium titanate

2002 J. Phys.: Condens. Matter 14 13635

(http://iopscience.iop.org/0953-8984/14/49/317)

INSTITUTE OF PHYSICS PUBLISHING JOURNAL OF PHYSICS: CONDENSED MATTER

J. Phys.: Condens. Matter **14** (2002) 13635–13641 PII: S0953-8984(02)53607-9

A computational study of twist boundary structures in strontium titanate

R Astala and P D Bristowe[1]

Department of Materials Science and Metallurgy, University of Cambridge, Pembroke Street, Cambridge CB2 3QZ, UK

E-mail: pdb1000@cus.cam.ac.uk

Received 18 September 2002
Published 29 November 2002
Online at stacks.iop.org/JPhysCM/14/13635

Abstract

A density functional plane-wave pseudopotential method is used to study various $\Sigma = 5$ (001) twist boundary models for strontium titanate. Results concerning the atom-level geometries and electronic structures are reported. The structures have varying SrO/TiO_2 ratios and their relative stabilities are discussed in terms of the SrO chemical potential. A twist boundary containing a Sr–O pair of vacancies is found to be exceptionally stable and have a low volume expansion and is a possible candidate for showing impurity segregation.

1. Introduction

Strontium titanate ($SrTiO_3$) is an electroceramic material that is often used in grain boundary barrier layer capacitors. The material has a high dielectric constant, which has been measured to be about 300 at room temperature [1]. In capacitor devices the polycrystalline material is doped with various oxide additives, e.g. Nb_2O_5 or Li_2O, in such a way that the grains become semiconducting and the grain boundaries become insulating. Thus it is important to understand the grain boundary segregation behaviour of the impurities and their effect on the electronic properties of the material. To do this, an understanding of the atom-level properties of the undoped boundaries must first be established. There have been several theoretical studies of tilt grain boundaries in $SrTiO_3$ including the $\Sigma = 3$ (111) twin boundary [2, 3] and the $\Sigma = 5$ (210) and (310) symmetric boundaries [4–9]. However, the properties of twist grain boundaries are poorly understood. In an investigation by Nomura *et al* [10], a $\Sigma = 5$ (001) twist boundary was studied using transmission electron microscopy and classical molecular dynamics. The experimental results showed that the twist boundary was atomistically sharp and had a periodicity related to the $\Sigma = 5$ coincidence site lattice (CSL). In addition, electrical conductivity measurements on this boundary together with $\Sigma = 1$ and 13 boundaries showed that they were electrically active. All the specimens had been doped with 0.05 wt% Nb. The

[1] Author to whom any correspondence should be addressed.

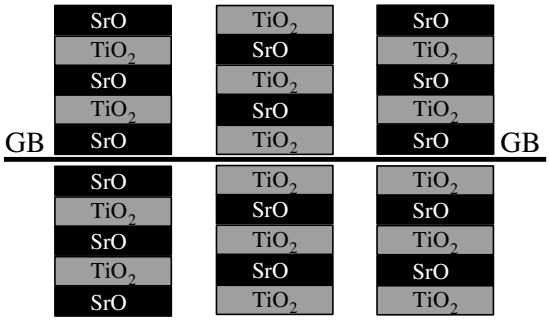

Figure 1. The (001) stacking sequences for three possible twist boundary structures having different local stoichiometries at the interface (GB). The top stack is rotated with respect to the bottom stack about [001].

computer simulations indicated that for a $\Sigma = 5$ interface bounded by TiO_2 and SrO layers, the energetically preferred structure was characterized by Ti and O ions in coincidence.

In this paper we present a first-principles computational investigation of the $\Sigma = 5$ twist boundary system which includes structural variants not considered previously. The structures have different local SrO/TiO_2 ratios, in-plane translations and point defect densities. The aim is to extract a set of possible low-energy structures that can then be used to study impurity segregation. The work extends our earlier investigation of twist boundaries to include various stoichiometries and defect complexes [11].

2. Model structures and computational methods

At room temperature, $SrTiO_3$ has the cubic perovskite structure which may be described as an alternating sequence of SrO and TiO_2(001) layers. The $\Sigma = 5$ (001) twist boundary can be created by dividing the structure along (001) and rotating one half of the crystal with respect to the other about [001] by $2\tan^{-1} 1/3 = 36.9°$. The resulting boundary structure has in-plane periodicity along [210] with a repeat distance of $\sqrt{5}a_0$, where a_0 is the bulk lattice constant. Three structural variants of the boundary can be defined depending on the layer termination at the interface. The boundary core can consist of two adjacent TiO_2 layers (T–T), two adjacent SrO layers (S–S) or one SrO layer and one TiO_2 layer (S–T). Only the latter structure retains the crystal stoichiometry. The different stacking possibilities are illustrated in figure 1. Further structural degrees of freedom include in-plane translations of the stacks and the creation of point defects. If only in-plane translations are considered, then for each of the three structural variants of the boundary the stacks can be shifted parallel to the interface to generate a set of distinct structures within the irreducible unit cell of the displacement shift complete (DSC) lattice. In this work, only translations corresponding to two high-symmetry points on this unit cell have been considered, one of which places like ions in coincidence and another which places unlike ions in coincidence. The former translational state is called the CSL structure and the latter is called the anti-CSL structure. For the T–T and S–S variants there exist one CSL and one anti-CSL structure. However, for the S–T variant, there is one CSL and two anti-CSL structures as shown in figure 2.

The creation of point defects in any of these boundary structures can relieve charge overlap, initiate reconstructions and allow for the possibility of local volume or density changes. Of the many defects that could be formed, only two are studied in this work: a Sr–O interstitial pair in the core of the T–T CSL boundary and a Sr–O vacancy pair in the core of the S–S CSL

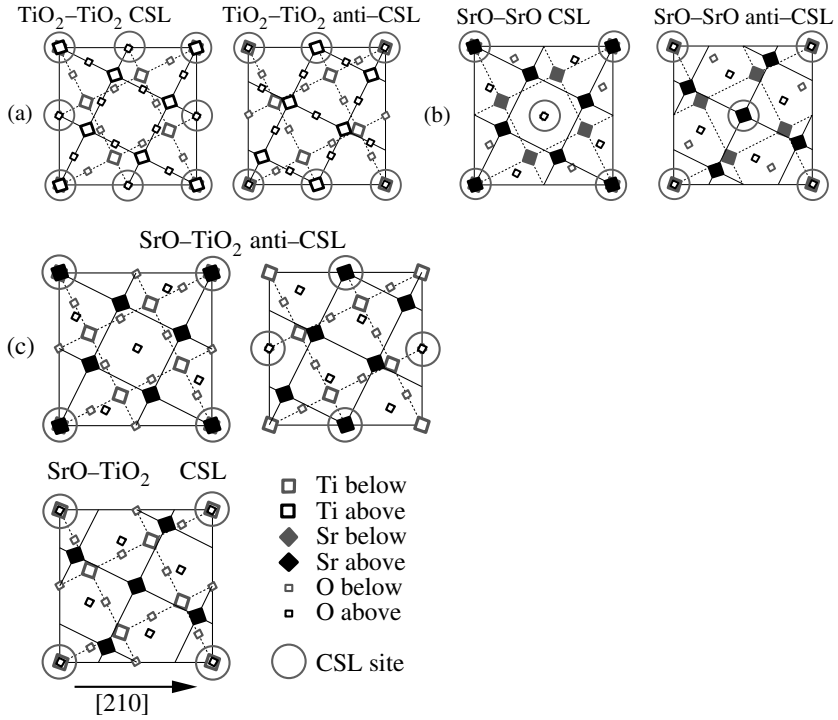

Figure 2. Plan views along [001] showing the seven distinct $\Sigma = 5$ geometries. (a) The TiO_2–TiO_2 interface, (b) the SrO–SrO interface, (c) the SrO–TiO_2 interface. One unit cell of the CSL is shown in each case.

boundary. For the interstitials, the O ion is placed between the Ti ions on the CSL sites and the Sr ion is placed on the eightfold-coordinated site separated from the O ion by $(1/2)[310]$. For the vacancies, one Sr ion and one O ion are removed from the CSL sites and the two remaining Sr and O ions are displaced normal to the boundary so as to occupy positions roughly between the SrO(001) layers at the boundary. The two defect structures are shown in figure 3. Note that adding or removing a Sr–O pair does not affect the overall charge neutrality of the boundary and therefore the defects are expected to have relatively low formation energies.

The twist boundaries are modelled using a density functional plane-wave pseudopotential method [12]. The GGS-PW91 functional is used to approximate the exchange–correlation energy and the ion cores are represented by Vanderbilt ultrasoft pseudopotentials available in the Cerius[2] software package [13, 14]. Accelrys CASTEP 4.2 software is used to perform the calculations [13]. The Brillouin zone is sampled using $2 \times 2 \times 1$ Monkhorst–Pack grids and the electron kinetic energy cut-off is set to 400 eV [15]. The calculations are performed using supercells and therefore each model contains two equivalent grain boundaries. The T–T model supercells consist of six TiO_2 and four SrO(001) layers while the S–S model supercells consist of six SrO and four TiO_2(001) layers. For the S–T boundaries, supercells consisting of five SrO and five TiO_2 layers are initially relaxed. Then the two structures of lowest energy, which are the anti-CSL variants, are relaxed using larger supercells consisting of six SrO and six TiO_2 layers. In all cases the lattice parameters and ionic coordinates are allowed to relax whilst the supercell angles are held fixed at 90°. In addition, bulk cells of $SrTiO_3$, SrO and TiO_2 (rutile), as well as TiO_2-and SrO-terminated (001) surface slab models of $SrTiO_3$ were relaxed as reference structures.

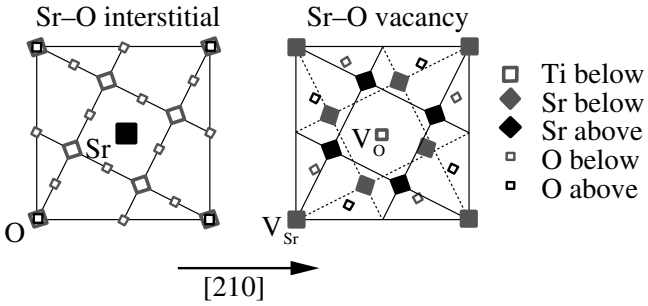

Figure 3. Plan views along [001] showing the TiO_2–TiO_2 CSL interface containing a Sr–O interstitial pair, and the SrO–SrO CSL interface containing a Sr–O vacancy pair.

Since the different twist boundary variants have different SrO/TiO_2 ratios, a comparison of their relative stabilities is not straightforward. However, the grain boundary energy σ can be written as a function of the SrO chemical potential $\mu(\mathrm{SrO})$ as

$$\sigma = \frac{E_{gb} - nE_0 - m\mu(\mathrm{SrO})}{2A} \tag{1}$$

where E_{gb} is the total energy of the supercell containing the grain boundary, E_0 is the energy of a single bulk $SrTiO_3$ unit, n is the number of TiO_2 units in the grain boundary model, m is the number of excess SrO units and A is the grain boundary area. The factor of $1/2$ stems from the presence of two grain boundaries in the supercell. The same expression can be applied to the grain boundaries containing point defects.

3. Results

The grain boundary energies per unit surface area were calculated using equation (1) and the results for the most stable structures are presented in figure 4. The slope of each curve indicates whether the structure is SrO or TiO_2 rich. It is seen that for the T–T, S–S and S–T variants of the $\Sigma = 5$ boundary, the translation states of lowest energy are the T–T anti-CSL, S–S CSL and S–T anti-CSL structures. All other translation states have higher energy and are not plotted in figure 4. However, the energies of the defect structures are shown and labelled Sr–O interstitial for the T–T CSL boundary and Sr–O vacancy for the S–S CSL boundary. By drawing the envelope of lowest-energy structures (full line), it is seen that the S–T Sr–O anti-CSL boundary and the S–S CSL vacancy boundary are the preferred structures over a wide range of SrO chemical potential. The T–T anti-CSL structure is also favoured but only in a very narrow range of chemical potential before bulk $SrTiO_3$ becomes unstable. The stability of each boundary with respect to dissociation into free (001) surfaces was also determined by computing their binding energies. Following our previous work [11], it was found that all variants of the boundary were stable with respect to dissociation into separate SrO or TiO_2 surfaces and had binding energies in the range 0.2–0.8 eV per unit area.

The relaxed structures of the low-energy variants had quite different characteristics. Figure 5 compares the S–S CSL and T–T anti-CSL structures where it is seen that the former is clearly more symmetric. The T–T anti-CSL structure exhibits a complicated pattern of relaxations in which the Ti and O ions attempt to optimize their coordination. The formation of Ti–O bonds across the boundary results in a relatively compact structure with a local volume expansion of 0.42 Å. The in-plane repeat distances increase slightly by 1–2%. The S–S CSL structure, on the other hand, has a larger volume expansion of 0.63 Å with in-plane repeat

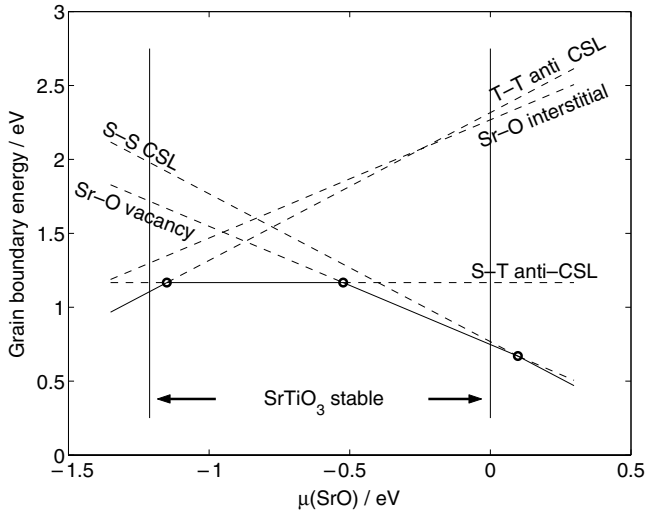

Figure 4. Grain boundary energies per unit area of various structural variants of the $\Sigma = 5$ twist boundary as a function of the SrO chemical potential. The unit of area is a (1×1) surface cell of $SrTiO_3$. Only the energies of the most stable T–T, S–S and S–T variants are shown. The chemical potential is scaled relative to bulk SrO and the vertical lines indicate threshold values beyond which bulk $SrTiO_3$ becomes unstable with respect to dissociation into either bulk SrO or bulk TiO_2 (rutile).

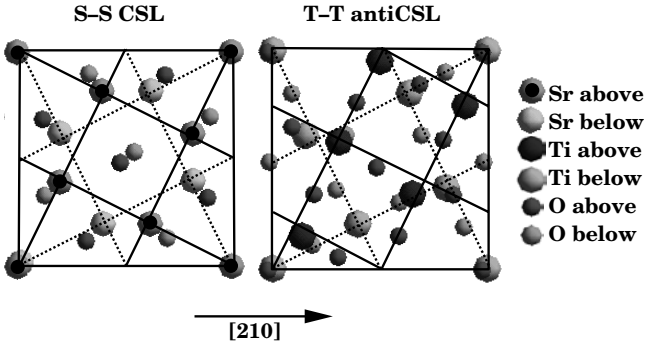

Figure 5. Plan views along [001] showing the relaxed structures of the SrO–SrO CSL interface and the TiO_2–TiO_2 anti-CSL interface. The grids indicate the unrelaxed lattice positions.

distances that slightly decrease. In this case the attraction between Sr and O ions across the boundary is counteracted by the strong repulsion between like ions on the CSL sites. Figure 6 shows a side view along $[\bar{1}20]$ of the relaxed structure of the S–T Sr–O anti-CSL variant. The SrO and $TiO_2(001)$ layers adjacent to the boundary become rumpled and two of the O ions in the SrO layer are strongly attracted towards the nearby Ti ions on the opposite side of the boundary. The Ti–O distance for these ions reduces to 1.82 Å whilst the distance to their original Ti neighbour increases to 2.65 Å. This boundary also has a large volume expansion of 0.84 Å although the in-plane repeat distances do not change much.

For the defect structures, the interstitial atoms incorporated into the T–T CSL structure remain very close to their initial positions between the two $TiO_2(001)$ layers. These layers became somewhat rumpled, but complex rearrangements similar to those observed in the T–T

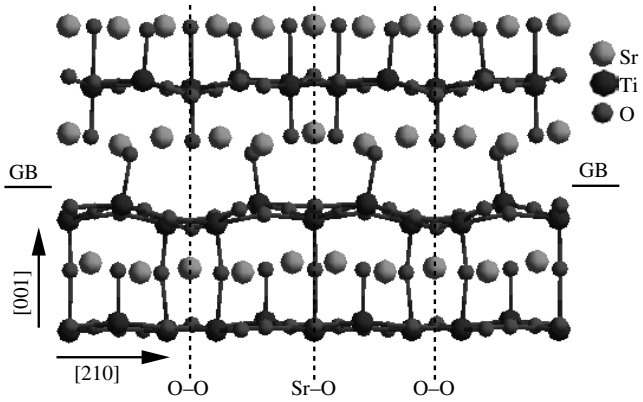

Figure 6. A side view along [$\bar{1}$20] parallel to the interface showing the relaxed structure of the $SrO–TiO_2$ Sr–O anti-CSL boundary. The positions of the Sr–O and O–O coincidence sites are indicated by dotted lines.

anti-CSL structure do not take place. The Ti–Ti distance across the boundary at the CSL sites where the O interstitial is located is 3.59 Å compared to 4.08 Å at the other sites. When the Sr–O vacancy pair is relaxed in the S–S CSL structure, the volume expansion reduces significantly as the like-ion repulsion at the CSL sites is relieved. The remaining Sr and O ions at the CSL sites prefer to relax away from their high-symmetry position between the SrO layers and both of them move towards the same SrO layer. The distance between the O ion and its Ti neighbour in the next TiO_2 layer becomes 1.86–1.90 Å indicating that the O ion has fully relaxed into the SrO plane.

4. Discussion and conclusions

Various structural variants of the $\Sigma = 5$ (001) twist boundary in $SrTiO_3$ have been studied using a density functional plane-wave pseudopotential method. The structural variants have different interfacial stoichiometries and in-plane translations. In addition, the formation of point defects in the boundary cores has been considered. The results indicate that the S–T Sr–O anti-CSL, T–T anti-CSL and S–S CSL with vacancy pair are the structures that are energetically preferred. Complex rearrangements of Ti–O bonds take place at the cores of the S–T and T–T boundary variants. However, when their electronic structures are analysed, no mid-gap states in the Kohn–Sham eigenenergy spectrum are observed, implying the absence of strong electrical activity associated with these boundaries. Even though the incorporation of a Sr–O interstitial pair into the T–T CSL boundary core is not energetically preferred, the resulting structure is stable and coherent. This is because the interstitial O ions complete the O octahedra surrounding the Ti ions at the CSL sites. The formation of a Sr–O vacancy pair in the core of the S–S CSL boundary reduces the boundary energy and the local volume expansion. This behaviour stems from the reduction in like-ion repulsion at the CSL sites. Interestingly, a similar arrangement of vacancies has been found to increase the stability of a $\Sigma = 5$ (001) twist boundary in NiO [16]. Furthermore, the S–S CSL boundary containing the vacancy pair has pockets of low valence charge density at its core as shown in figure 7. Therefore this particular structural variant of the boundary in $SrTiO_3$ appears to be a promising candidate for use in the study of segregation effects since it has free volume to accommodate impurities and its electronic structure is sufficiently different from that of the bulk crystal to allow soft electron-level relaxations to take place.

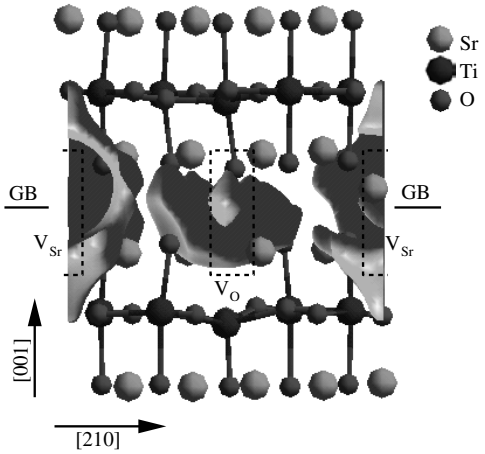

Figure 7. The valence charge isosurface at the grain boundary core of the SrO–SrO CSL structure containing a Sr–O vacancy pair. The structure is viewed along [$\bar{1}$20] parallel to the interface and the rectangle indicates the location of the vacancies. The charge density is calculated using a $3 \times 3 \times 1$ Monkhorst–Pack grid. The clouds indicate pockets of low charge density ($<0.03\ e\ Å^{-3}$).

Acknowledgments

This work was supported by the Finnish Academy of Sciences and Letters-Väisälä Foundation and by the UK EPSRC. The resources of the Cambridge University High Performance Computing Facility have been used to perform the calculations.

References

[1] Neville R C, Hoeneisen B and Mead C A 1972 *J. Appl. Phys.* **43** 2124
[2] Kienzle O, Exner M and Ernst F 1998 *Phys. Status Solidi* a **166** 57
[3] Hutt S, Köstlmeier S and Elsässer C 2001 *J. Phys.: Condens. Matter* **13** 3949
[4] Kim M, Duscher G, Browning N D, Sohlberg K, Pantelides S T and Pennycook S J 2001 *Phys. Rev. Lett.* **86** 4056
[5] Mo S-D, Ching W Y, Chisholm M F and Duscher G 1999 *Phys. Rev.* B **60** 2416
[6] Rodrigues R P, Chang H, Ellis D E and Dravid V P 1999 *J. Am. Ceram. Soc.* **82** 2385
[7] Rodrigues R P, Ellis D E and Dravid V P 1999 *J. Am. Ceram. Soc.* **82** 2395
[8] Chang H, Rodrigues R P, Xu J-H, Ellis D E and Dravid V P 1997 *Ferroelectrics* **194** 249
[9] Chang H, Lee J D, Rodrigues R P, Ellis D E and Dravid V P 1998 *J. Mater. Synth. Process.* **6** 323
[10] Nomura M, Ichinose N, Yamaji K, Haneda H and Tanaka J 1999 *J. Electroceram.* **4:S1** 91
[11] Astala R and Bristowe P D 2002 *Perovskite Materials (Mater. Res. Soc. Symp. Proc. vol 718)* ed K Poeppelmeier, A Navrotsky and R Wentzcovitch (Pittsburgh, PA: Materials Research Society) p 77
[12] Payne M C, Teter M P, Allan D C, Arias T A and Joannopoulos J D 1992 *Rev. Mod. Phys.* **64** 1045
[13] *Cerius*^{2} *User Guide* 1999 MSI/Accelrys
[14] Vanderbilt D 1990 *Phys. Rev.* B **41** 7892
[15] Monkhorst H J and Pack J D 1974 *Phys. Rev.* B **13** 5188
[16] Tasker P W and Duffy D M 1983 *Phil. Mag.* A **47** L45